catalysts

MDPI

Article

Improvement of NH_3-SCR Performance by Exposing Different Active Components in a VCeMn/Ti Catalytic System

Shifei Gu [1,2], Chengheng Huang [1,2], Xiaorong Han [1,2], Qiuju Qin [1,2], Donghai Mo [1,2], Chen Li [1,2], Yuhua You [1,2], Lihui Dong [1,2] and Bin Li [1,2,*]

[1] A State Key Laboratory of Featured Metal Materials and Life-Cycle Safety for Composite Structures, Guangxi University, Nanning 530004, China; 2214301014@st.gxu.edu.cn (S.G.); 2214301028@st.gxu.edu.cn (C.H.); 2214301019@st.gxu.edu.cn (X.H.); 1914301051@st.gxu.edu.cn (Q.Q.); 2114301103@st.gxu.edu.cn (D.M.); 2204200247@st.gxu.edu.cn (Y.Y.); 2114301035@st.gxu.edu.cn (C.L.); donglh@gxu.edu.cn (L.D.)

[2] Guangxi Colleges and Universities Key Laboratory of Applied Chemistry Technology and Resource Development, School of Chemistry and Chemical Engineering, Guangxi University, Nanning 530004, China

* Correspondence: binli@gxu.edu.cn; Tel.: +86-139-7881-1632

Abstract: The physicochemical properties of active components play a key role in enhancing catalytic performance. In multi-component catalysts, different components offer a wide range of structural possibilities and catalytic potential. However, determining the role of specific components in enhancing efficiency may be blurry. This study synthetized a range of catalysts with various metal compositions on their external surfaces to investigate their catalytic activity on NH_3-SCR. The V/CeMn/Ti catalysts exhibited exceptional catalytic efficiency and strong tolerance to SO_2 during the SCR process. In the system, Mn and Ce facilitated electron transfer during the catalytic removal of NO_x. As an assisting agent, increased the number of active species and acidic sites, playing a crucial role in oxidizing NO to NO_2 and facilitating the denitrogenation reaction process at low temperatures. Further studies showed that the three ingredients exhibited unique adsorbent behaviors on the reacting gases, which provided different catalytic possibilities. This work modeled the particular catalysis of V and Ce (Mn) species, respectively, and offers experimental instruction for improving the activity and excellent tolerance to SO_2 by controlling active ingredients.

Keywords: low-temperature NH_3-SCR of NO; In-situ DRIFTS; Redox property; surface acidity; vanadia-based catalysts

Citation: Gu, S.; Huang, C.; Han, X.; Qin, Q.; Mo, D.; Li, C.; You, Y.; Dong, L.; Li, B. Improvement of NH_3-SCR Performance by Exposing Different Active Components in a VCeMn/Ti Catalytic System. *Catalysts* **2024**, *14*, 131. https://doi.org/10.3390/catal14020131

Academic Editor: Rufino M. Navarro Yerga

Received: 9 January 2024
Revised: 31 January 2024
Accepted: 5 February 2024
Published: 7 February 2024

1. Introduction

NH_3-SCR is the most prevalent technology for effectively removing NO_x [1,2]. Currently, several types of catalysts are widely used for the removal of NO_x, including ion-exchanged zeolite catalysts, V-based catalysts, and other oxide catalysts [3,4]. V-based catalysts are widely used for their superior SO_2 resistance [5–7]. V_2O_5-WO_3(MoO_3)/TiO_2 catalysts are commonly used for commercial applications. However, such catalysts are unsuited for low-temperature flue gases in industries such as those of glass and steel, as they have weak low-temperature NH_3-SCR activity and a confined operating temperature window [1,5,8,9]. While high V-loads can effectively enhance catalytic activity at low temperatures, they are also linked to several issues, including enhanced oxidation of SO_2 to SO_3, a narrow operating temperature window, poor alkali resistance, low N_2 selectivity, and toxicity of V [1,6]. Therefore, the development of new V-based catalysts with a low vanadium loading and outstanding activity at low temperatures is important.

Anatase TiO_2 was extensively used in commercial V-based catalysts for many years because of its outstanding tolerance to SO_2 and its ability to improve the dispersion of vanadium-based materials [1,6]. Modifying the supports can effectively enhance the low-temperature activity and SO_2 durability of V-based catalysts [7]. A loaded $V_2O_5/Ce_{1-x}Ti_xO_2$ catalyst exhibited better NO_x conversion and SO_2 resistance than those of V_2O_5/TiO_2 or

V_2O_5/CeO_2 at low temperatures after CeO_2 was doped into TiO_2, which was attributed to the improved surface dispersion of vanadium-based substances and higher reducibility [8]. According to the above results, V-oxides loaded on TiO_2-containing mixed oxides consistently exhibited higher reactivity and excellent SO_2 resistance in comparison with those loaded on pure Ti oxides. Additionally, mixed oxide loading may impact the surface active components. Therefore, further exploration of catalysts for low-temperature NH_3-SCR reactions is necessary. Manganese-doped or loaded mixed oxides appear to be among the most prominent material candidates for reducing the temperature required for the NH_3-SCR reaction [10–12]. The redox cycle of superficial Mn^{3+}/Mn^{4+} or Mn^{2+}/Mn^{3+} in manganese oxides (MnO_x) is known for its high catalytic activity. Mn^{3+}/Mn^{4+} or Mn^{2+}/Mn^{3+} in manganese oxides (MnO_x) is known for its high catalytic activity. It has been shown that Mn-Ce/TiO_2 [13], MnO_x/CeO_2/AC [14], Mn-Ce-V/AC [15], and MnO_x/SAPO-34 [16] have outstanding low-temperature NH_3-SCR activity. For example, Yang et al. [17] investigated a MnO_x-CeO_2 catalyst synthesized through co-precipitation, which achieved a NO conversion of 95% at 150 °C. Huang and colleagues discovered that 10 wt% MnO_x loaded on multi-walled carbon nanotubes (MWCNTs) in the range of 180–240 °C exhibited the best NO conversion [18]. However, the above debate was mainly concerned with activating NH_3 and NO on the surface catalysts, but the functions of the different active ingredients in complicated catalytic systems remain unclear. Inspired by the above studies, by using graded impregnation to load V, Ce, and Mn on a TiO_2 support, it is possible to extend the operating temperature window of the catalysts, improve the activity of NH_3-SCR at low temperatures, and increase the resistance to H_2O/SO_2. This multicomponent approach not only optimizes the chemico-physical properties but also influences the adsorption and conversion of reactive gases via different pathways [19,20]. However, the roles of the components in the NH_3-SCR reaction within such a complex system are intricate. Hence, it is essential and worthwhile to elucidate the roles of various ingredients in complicated catalytic systems.

In this study, a stepwise co-impregnation method was used to synthesize a series of catalysts with different exposed active components. The graded catalysts were characterized to investigate the effects of exposure to different active components on the NH_3-SCR performance. Finally, we propose a possible mechanism for the enhancement of the SCR performance of V/MnCe/Ti catalysts. This study provides a guide to the experimental investigation of the catalytic potential of multi-composite V-based catalysts by elucidating the functions of various active species in catalysis.

2. Results and Discussion

2.1. Catalytic Performance

Figure 1a displays the results for the activity of various catalysts. The NO conversion decreased in the sequence of CeMn/V/Ti > V/CeMn/Ti > VCeMn/Ti at temperatures between 100 and 175 °C. This suggested that at low temperatures, the Ce (Mn) exposed on the outer surface of the catalysts was the dominant active species. Nevertheless, as the reaction temperature increased, the NO conversion was increased with respect to that of V/CeMn/Ti, and there was >90% NO conversion over a broad temperature range of 175–325 °C. With the further increase in the reaction temperature, the NO conversion slightly decreased because of the partial oxidation of NH_3 [20]. Moreover, the NO conversion of the V/CeMn/Ti catalyst was higher than that of the CeMn/V/Ti and VCeMn/Ti catalysts at 175–325 °C, which indicated the synergistic effect between V and Ce (Mn). In summary, the V/CeMn/Ti catalysts had better NO conversion over the entire temperature range, which may have been associated with the good dispersion and reducibility of the active species of V exposed on the outer surface of the catalyst at medium and high temperatures.

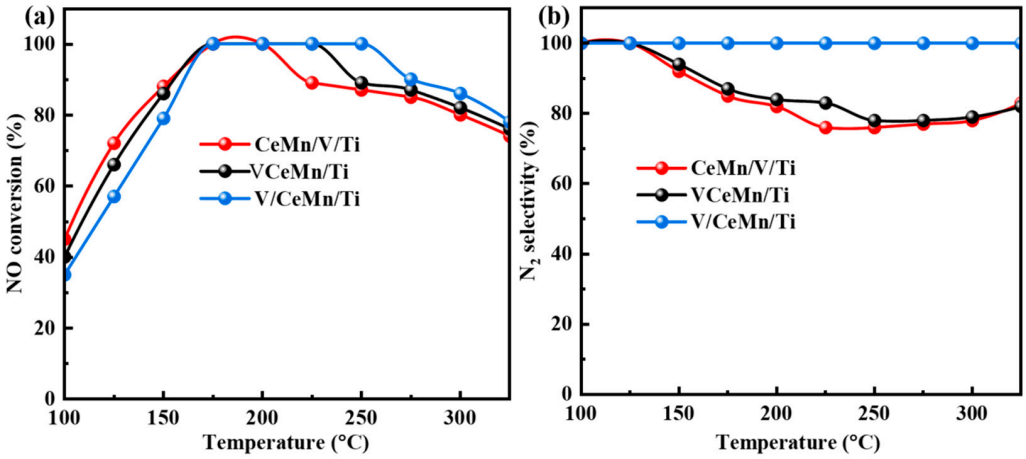

Figure 1. Catalytic performance of the catalysts. (**a**) NO conversion; (**b**) N_2 selectivity (condition: NO = NH_3 = 500 ppm, O_2 = 5 vol%).

The N_2 selectivity results of the catalysts are displayed in Figure 1b. Compared with other previously reported high-activity catalysts, the V/CeMn/Ti, CeMn/V/Ti, and VCeMn/Ti catalysts exhibited high N_2 selectivity over the entire range of testing temperatures, and for the CeMn/V/Ti and VCeMn/Ti samples, the N_2 selectivity decreased from 100% to 80% from 150 to 325 °C, which may have been the result of the increase in the test temperature increases, while the NH_3 adsorbed on the CeMn/V/Ti and VCeMn/Ti catalysts was more easily oxidized by O_2, leading to the production of N_2O. Interestingly, the N_2 selectivity of the V/CeMn/Ti catalyst was maintained at 100% throughout the tested temperature range. N_2O is one of the byproducts produced in the over-oxidation of NH_3 at high temperatures. The above results indicate that the N_2 selectivity was improved and the non-selective oxidation of NH_3 was significantly suppressed when V was exposed to the outer surface of the catalysts.

H_2O and SO_2 Tolerance Tests

The catalysts' resistance to H_2O and SO_2 was tested at 225 °C, as illustrated in Figure 2. The introduction of 5 vol.% H_2O into the reaction system slightly reduced the activities of the V/CeMn/Ti and CeMn/V/Ti catalysts. The reduction could be explained by the competitive absorption of NH_3 and H_2O [21]. When the H_2O was removed, the NO_x conversion was restored, suggesting that the impact of H_2O was reversible. However, the slight increase in NO_x conversion for the VCeMn/Ti catalysts suggested that they were more effective in reducing NO_x with NH_3 in the presence of H_2O. This is crucial for practical applications. The introduction of 50 ppm SO_2 caused a decline in the NO_x conversion of all catalysts, which may have been due to the reaction of SO_2 with certain metal sites in the catalysts to form metal sulphates, which disrupted the redox SCR pathway of the catalysts, resulting in their irreversible inactivation [3,22]. If active sites are covered by surface metal sulfates or accumulated NH_4HSO_4 and become inactive, the catalyst lacks sufficient active sites [19]. The introduction of H_2O + SO_2 simultaneously for 2 h led to a significant decrease in NO conversion for all catalysts, which was attributed to the following: Firstly, there was a competitive adsorption of SO_2 and excess H_2O (5 vol%, 50,000 ppm) with NH_3 and NO; secondly, SO_2 + H_2O could react directly with the reducing NH_3 gas to produce ammonium bisulfate (NH_4HSO_4), which tended to inhibit the activity of the sites or be deposited on the surface of the catalysts. The NO_x conversion of all catalysts did not return to the original values when SO_2 and H_2O were removed, indicating that the impact of SO_2 + H_2O on the catalysts was irreversible. The V/CeMn/Ti catalyst had superior tolerance for SO_2 + H_2O compared to that of the CeMn/V/Ti and VCeMn/Ti catalysts, which may have been because V covered the outside surface of the activated Ce (Mn) to prevent SO_2 from interacting with the active compounds.

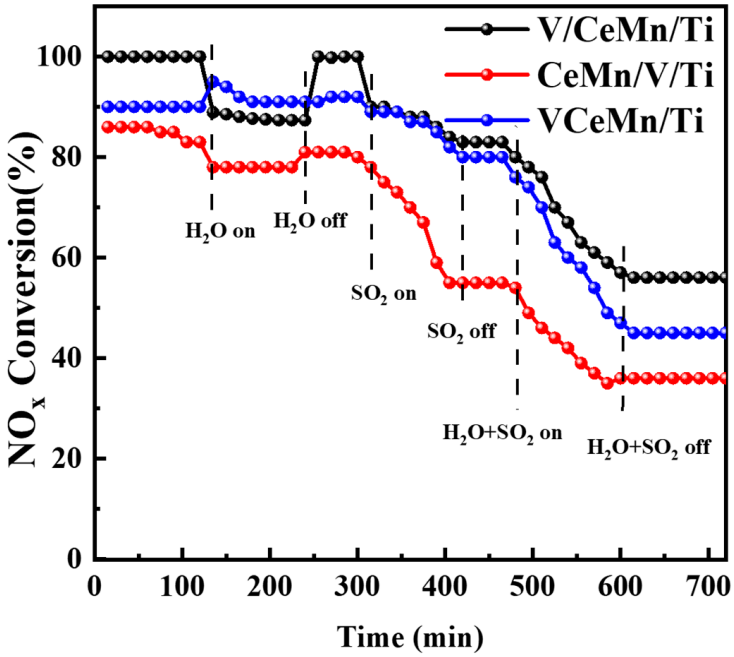

Figure 2. Comparison of H_2O and SO_2 resistance (reaction conditions: 220 °C, NO = NH_3 = 500 ppm, O_2 = 5 vol%, H_2O = 5 vol%, SO_2 = 50 ppm).

2.2. Structure and Morphology

The crystal structure of the catalysts was the subject of X-ray diffraction measurements, as shown in Figure 3. It was evident that the catalysts had similar 2θ diffraction locations but with various diffraction strengths. The diffraction peaks of 2θ at 25.2°, 37.6°, 48.2°, 52.9°, 55.3°, 62.6°, 68.7°, 70.4°, and 75.1° corresponded to the (101), (004), (200), (105), (211), (204), (116), (220), and (215) anatase TiO_2 facets, respectively [21]; the diffraction peaks of 2θ at 27.5°corresponded to the rutile TiO_2, and the diffraction peaks of the three catalysts at 2θ = 28.5° were the typical diffraction peaks of MnO_2. The Scherrer equation was used to calculate the particle size of MnO_2, and the particle sizes of MnO_2 in the VCeMn/Ti, CeMn/V/Ti, and V/CeMn/Ti catalysts were 13.1472, 13.1480, and 13.1483 nm. The VCeMn/Ti catalyst had the smallest particle size, which indicated that the particles were reduced and the relative surface area was increased, which was in accordance with the conclusions from BET (Figure S1). No distinct diffraction peaks corresponding to the oxides of V and Ce were observed in the catalysts, which suggested that the doped metal oxides were present in an altitudinally dispersed state, which facilitated mutual contact with the activated ingredients and was conducive to strong reactions between the metal oxides [23]. SEM was used to observe the morphology of the catalysts, as shown in Figure S2. The morphologies of the three catalysts were similar, consisting of nanoparticles of varying sizes [23]. The results showed that the morphology of the catalysts was not affected by the order in which the active ingredients were loaded. The relevant BET surface areas and pore size distributions are summarized in Table 1; the catalysts exhibited "IV" adsorption–desorption isotherms with H3-type hysteresis loops, and their pore sizes were predominantly distributed between 2 and 50 nm, suggesting that the catalysts were formed from mesoporous structures [24,25]. The BET surface area declined in the order of V/CeMn/Ti ≈ CeMn/V/Ti > VCeMn/Ti, and the specific surface area of the catalysts that were synthetized through step-impregnation was larger than that of the catalysts that were synthetized through one-step impregnation. This could be attributed to the aggregation of MnO_2 on the VCeMn/Ti catalyst during its preparation, leading to a reduction in its specific surface area (Figure S1).

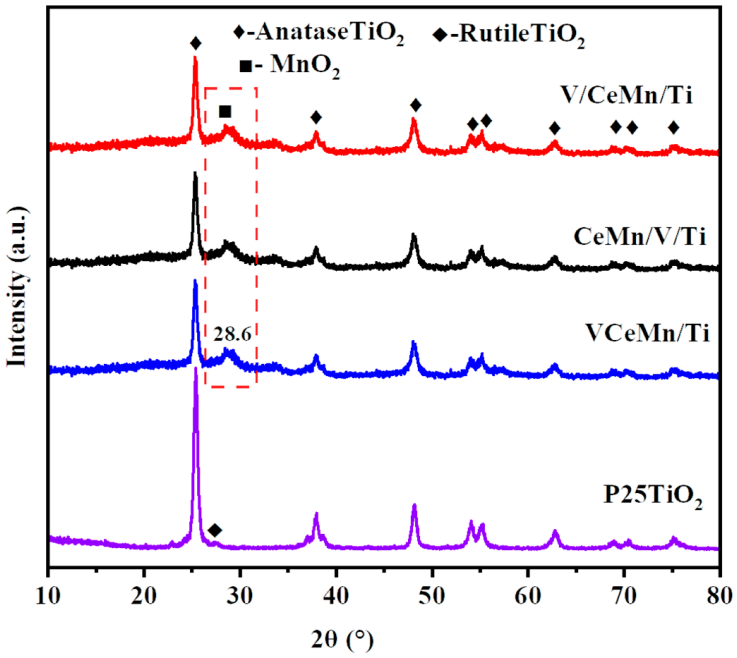

Figure 3. Catalysts' XRD patterns.

Table 1. Textural properties of all catalysts.

Samples	BET ($m^2 \cdot g^{-1}$)	Pore Volume ($cm^3 \cdot g^{-1}$)	Pore Size (nm)
V/CeMn/Ti	52	0.17	11.29
CeMn/V/Ti	51	0.13	11.00
VCeMn/Ti	38	0.15	10.12

2.3. Raman Analysis

The structural characteristics of V and Ce were studied with Raman spectroscopy. As shown in Figure 4, the weakly adsorbed peak at about 168 cm^{-1} was attributed to the B_{1g} mode of anatase TiO_2 [26,27]. No TiO_2 peaks were detected for the VCeMn/Ti catalysts because of the presence of more of the MnO_2 crystal phase on the surface, resulting in a weakening of its peak intensity. The results were consistent with those of XRD, and a prominent peak was centered at 450 cm^{-1}, which suggested that CeO_2 was present in the form of microcrystals [28,29], though this was undetectable in the XRD analysis. The peaks at 230 and 685 cm^{-1} were attributed to oxygen vacancies because of the presence of Ce^{3+} [29,30]. Oxygen vacancies enhance oxygen uptake and improve the efficiency of conversion between Ce^{3+} and Ce^{4+} [30]. Moreover, the strongest peak strengths were found for the V/CeMn/Ti catalysts, suggesting the presence of more oxygen vacancies that would promote NO oxidation and further facilitate the NH_3-SCR reaction [31]. The peak at 1005 cm^{-1} was attributed to the monomeric V species. The peak at 960 cm^{-1} was attributed to the polymeric V species; according to the literature [32], the polymeric state of vanadium exhibits significantly higher activity than that of its monomeric state. Interestingly, the band at 960 cm^{-1} was the strongest for the V/CeMn/Ti catalyst, indicating that the V/CeMn/Ti catalyst had the best SCR performance, which was consistent with the results for the activity.

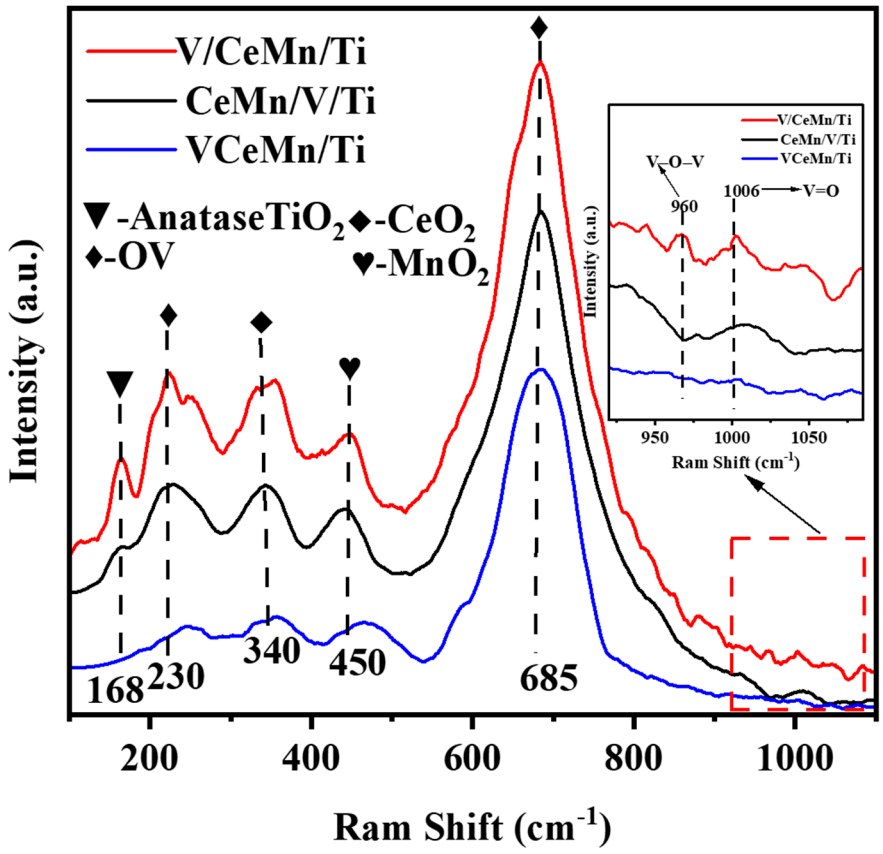

Figure 4. Raman spectroscopy of the catalysts.

2.4. Acidic Site Distribution (NH_3-TPD)

A catalyst's surface acidity can influence the adsorption of NH_3 and further impact the catalytic reaction. Figure 5a displays the NH_3-TPD results. All catalysts were fitted into four desorption peaks in the range of 100–700 °C. The four peaks were the physical adsorption peak (at 100–150 °C; corresponding peak I) and the peaks of NH_3 desorption on weak acids (Aw: 150–350 °C; corresponding peak II), medium-strong acids (Am: 400–550 °C; corresponding peak III), and strong acids (As: 550–700 °C; corresponding peak IV) [33,34]. Previous studies have reported [35,36] that NH_4^+ ions adsorbed at weak acid sites have lower thermal stability than that of NH_3 adsorbed at strong acid sites. The peaks of desorption at lower temperatures were caused by the desorption of NH_3 from the weak acid sites, and the peaks at higher temperatures were due to the desorption of NH_3 from strong acid sites. Figure 5b displays the number of distinct acid sites. The analysis of the peak areas showed that the VCeMn/Ti catalyst had the smallest amount of acid compared to the other catalysts. However, the V/CeMn/Ti catalysts had a greater amount of acid—especially weak acids—than the CeMn/V/Ti and VCeMn/Ti catalysts. Therefore, the acidity of the catalyst was increased when the active component V was exposed to the outer surface of the catalyst.

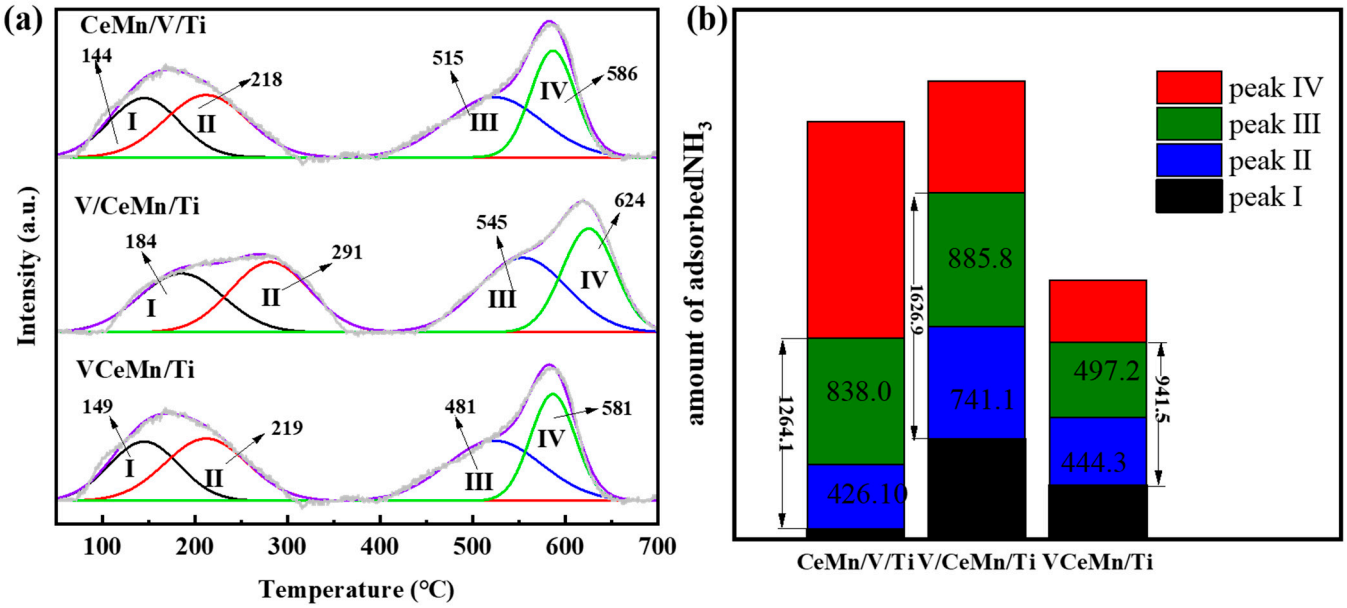

Figure 5. (**a**) NH_3-TPD; (**b**) corresponding NH_3 consumption.

2.5. The Oxidation–Reduction Properties of the Catalysts

The O_2-TPD of the catalysts is shown in Figure 6a. Three O_2 desorption peaks were observed in the range of 100–400 °C, and they were attributed to physically adsorbed oxygen (O_p, around 200 °C), chemically adsorbed oxygen (O_c, around 250 °C), and lattice oxygen (surface lattice oxygen O_s), respectively. The V/CeMn/Ti catalyst had the smallest adsorption capacity for O_s, indicating that it had more oxygen vacancies, which led to more chemisorbed oxygen and was consistent with it having more O_c, which helped to upgrade its catalytic properties. The desorption peaks of the VCeMn/Ti catalyst were weaker, suggesting that it had a poorer capacity for storing oxygen. The area of the O_c peaks of the V/CeMn/Ti catalyst was much larger than those of the CeMn/V/Ti and VCeMn/Ti catalysts, which indicated that the oxygen storage capacity of the V/CeMn/Ti catalysts was much larger than that of the CeMn/V/Ti and VCeMn/Ti catalysts, and the exposure of active V species to the outer surface of the catalysts significantly increased the oxygen storage capacity, which was consistent with the Raman results.

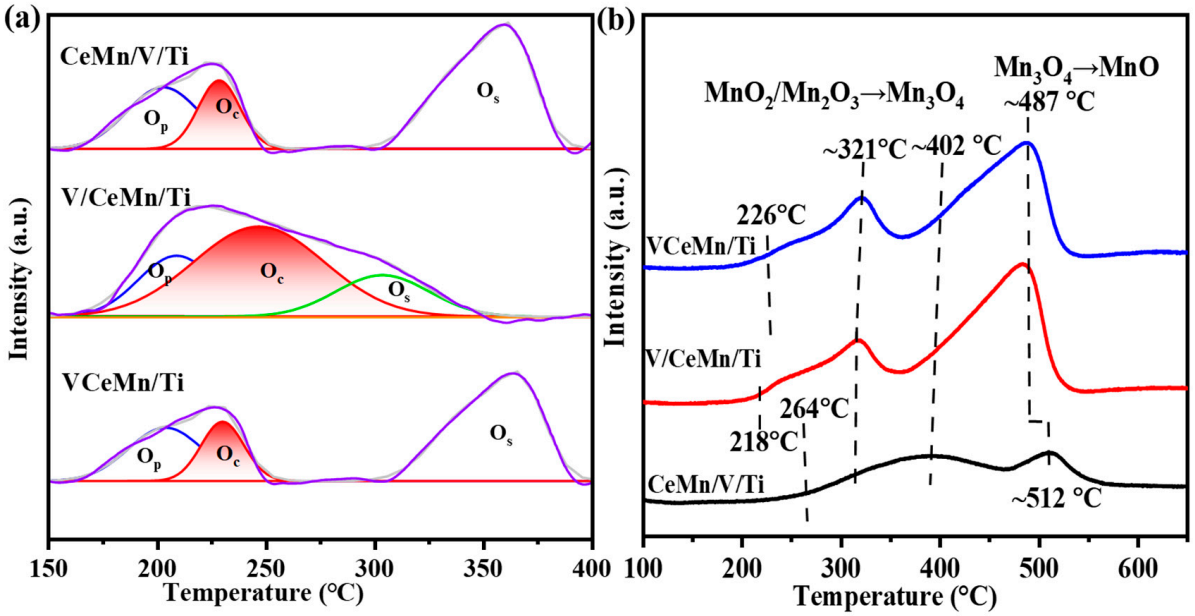

Figure 6. (**a**) O_2-TPD and (**b**) H_2-TPR for CeMn/V/Ti, V/CeMn/Ti, and VCeMn/Ti.

The reductive characteristics of the catalysts were determined through H_2-TPR experiments, as shown in Figure 6b. The catalysts had two large reduction peaks; the initial broad peak at 200 °C–400 °C was attributed to $MnO_2 \rightarrow Mn_2O_3 \rightarrow Mn_3O_4$, and the second broad peak at 450 °C–550 °C was attributed to $Mn_3O_4 \rightarrow MnO$ [37–39]. The reduction peak onset temperature of the V/CeMn/Ti catalyst was lower than those of the CeMn/V/Ti and VCeMn/Ti catalysts. This suggested that the VO-V species in the polymeric state improved the interactions between Mn and Ce, which made the active substances easier to reduce and greatly improved the surface oxygen mobility, thus improving the catalyst's low-temperature activity [40]. There have been reports that this synergistic effect can lead to changes in the electron structures of the catalyst surface, as well as the generation of many oxygen vacancies, which facilitate the diffusion of surface oxygen into the bulk phase. These features contributed to the performance of NH_3-SCR [41,42].

2.6. XPS Analysis

X-ray photoelectron spectroscopy (XPS) was used to study the chemical state of the surface elements of the catalysts. Figure 7 reveals the XPS spectra of Mn 2p, Ce 3d, O 1s, and V 2p, and the percentages are shown in Table 2. Figure 7a exhibits two dominant peaks of Mn 2p3/2 and Mn 2p1/2 at 633 eV and 665 eV. The Mn 2p3/2 spectrum was segmented into three distinctive peaks, which were assigned to Mn^{2+} (~640.7 eV), Mn^{3+} (~641.6V), and Mn^{4+} (~643.6 eV) [43,44]. Table 2 shows that the ratio of Mn^{4+}/Mn^{2+} was significantly higher in V/CeMn/Ti (42.7%) than in CeMn/V/Ti (25.3%) and VCeMn/Ti (29.6%). Manganese oxide species with a higher valence state exhibited greater redox activity on Mn-based catalysts [44]. Furthermore, Mn^{4+} was shown to expedite the conversion of NO into NO_2 and enhance the SCR reaction via the "fast SCR" pathway, which was in agreement with the catalytic performance of the catalysts.

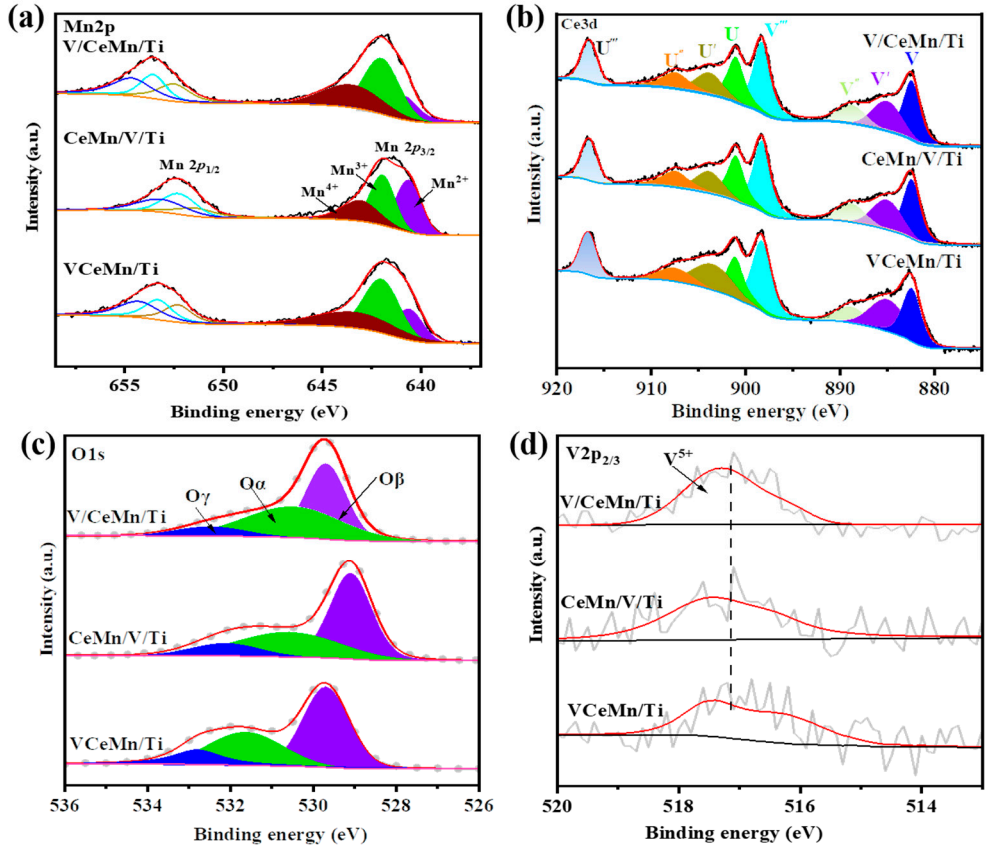

Figure 7. XPS for the (**a**) Mn 2p, (**b**) Ce 3d, (**c**) O 1s, and (**d**) V 2P orbitals of the catalysts.

Table 2. The XPS results for O 1s, Mn 2p, and Ce 3d were compared for the different catalysts.

Samples	Mn^{4+}/Mn^{n+} (%)	$Ce^{4+}/(Ce^{4+} + Ce^{3+})$ (%)	O_α (%)
V/CeMn/Ti	42.7	79	49
CeMn/V/Ti	25.3	72	35
VCeMn/Ti	29.6	60	33

As shown in Figure 7b, the Ce 3d XPS spectra of the catalysts were fitted with eight peaks: V (882.3 eV), V′ (884.2 eV), V″ (889.0 eV), V‴ (899.2 eV), U (901.2 eV), U′ (903.4 eV), U″ (906.5 eV), and U‴ (916.6 eV), which corresponded to four couples of spin–orbit doubles [44,45]. The peaks marked V and U belonged to the spin–orbit fractions of Ce3 $d_{5/2}$ and Ce $3d_{3/2}$, respectively. The peaks denoted by V, V″, V‴, U, U″, and U‴ were attributed to characteristic peaks of Ce^{4+}, whereas the peaks labeled V′ and U′ are attributed to Ce^{3+} [46–48]. The Ce 3d XPS spectra indicated the coexistence of Ce^{3+} and Ce^{4+} species on the catalysts, which were already shown to produce charge imbalances, oxygen vacancies, and unsaturated chemical bonds on the catalysts' exterior, which were helpful for the formation of chemically adsorbed oxygen on the catalyst surface [44,46]. As demonstrated in Table 2, a higher proportion of Ce^{4+} (79%) was observed when the active V species were exposed to the outermost layer of the catalyst, indicating that V could boost the $Mn^{3+} + Ce^{4+} \leftrightarrow Mn^{4+} + Ce^{3+}$ oxidation–reduction cycle in the catalysts that were prepared in a stepwise manner, which corresponded to the results of O_2-TPD.

Figure 7c shows the XPS spectra of O 1s. The deconvolution of the O 1s spectra produced three distinct peaks: a peak with a bond energy of about 528.9–530.4 eV was attributed to lattice oxygen (O^{2-}, supplied as O_β); a peak with a binding energy of 530.9–532.9 eV was attributed to the oxygen that was chemically adsorbed on the surface (O_2^{2-} or O^-, supplied as O_α); meanwhile, a peak with a bond energy of about 529.9–535.6 eV was assigned to species of oxygen in hydroxyl groups (marked as O_γ) [49]. It was confirmed that the catalytic activity of oxygen adsorbed on a surface was better than that of lattice oxygen due to its high migration rate, which plays an important role in oxidation reactions [13]. As shown in Table 2, the percentage of O_α on the V/CeMn/Ti catalyst was higher than that on the CeMn/V/Ti and VCeMn/Ti catalysts, which suggested that the V/CeMn/Ti catalysts produced more oxygen vacancies that could promote the properties of NH_3-SCR. The V 2p XPS results are shown in Figure 7d. The active V species in the three catalysts were predominantly in the form of V^{5+}.

On the basis of the analysis of the above characterization results, a possible redox cycle on the V/CeMn/Ti catalyst was proposed. As shown in Figure 8, in the primary impregnation products of CeMn/Ti, there was a redox cycle in the form of $Mn^{4+} + Ce^{3+} \leftrightarrow Mn^{3+} + Ce^{4+}$. The coexistence of Ce^{3+} and Ce^{4+} species was shown to generate charge imbalances, oxygen vacancies, and unsaturated chemical bonds at the catalyst surface, and it facilitated the formation of chemisorbed oxygen on the catalyst surface [44,46]. The exposure of V to the outer surface of CeMn/Ti significantly improved the redox cycle and electron transfer, and it promoted NO/NH_3 adsorption/activation.

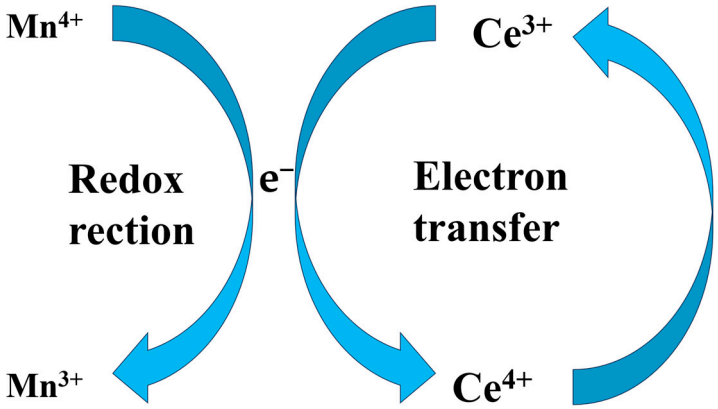

Figure 8. Schematic diagram of redox cycling for the V/CeMn/Ti catalysts.

2.7. In Situ DRIFTS

In this study, in situ DRIFTS was performed to illustrate the interaction of the surface active sites of NH_3 and NO intermediates on the catalysts.

2.7.1. NH_3 Adsorption–Desorption

In situ DRIFTS was conducted on three catalysts to elucidate their excellent performance. As shown in Figure 9, the peak located at ~1456 cm^{-1} was attributed to NH_4^+ ions adsorbed at the B-acid site. The peaks that emerged at ~1153 cm^{-1} and ~1293 cm^{-1} were assigned to NH_3 species that were absorbed at the L-acid site [50]. The peaks observed at about ~1078 cm^{-1} and ~1530 cm^{-1} were assigned to NH_2^- species that were absorbed on the L-acid site and NH_2 coordinate to the L-acid [51]. According to these results, L-acid and B-acid coexisted in the catalysts. Upon contrasting the peak intensities of all catalysts, it was discovered that the strongest peak intensities were those of NH_4^+ and NH_3 species absorbed on the B-acid sites and L-acid sites in the V/CeMn/Ti catalyst, which implied that the V/CeMn/Ti catalyst had the strongest acidic sites when V was exposed to the outer surface of the catalyst, and this was consistent with the results for the activity.

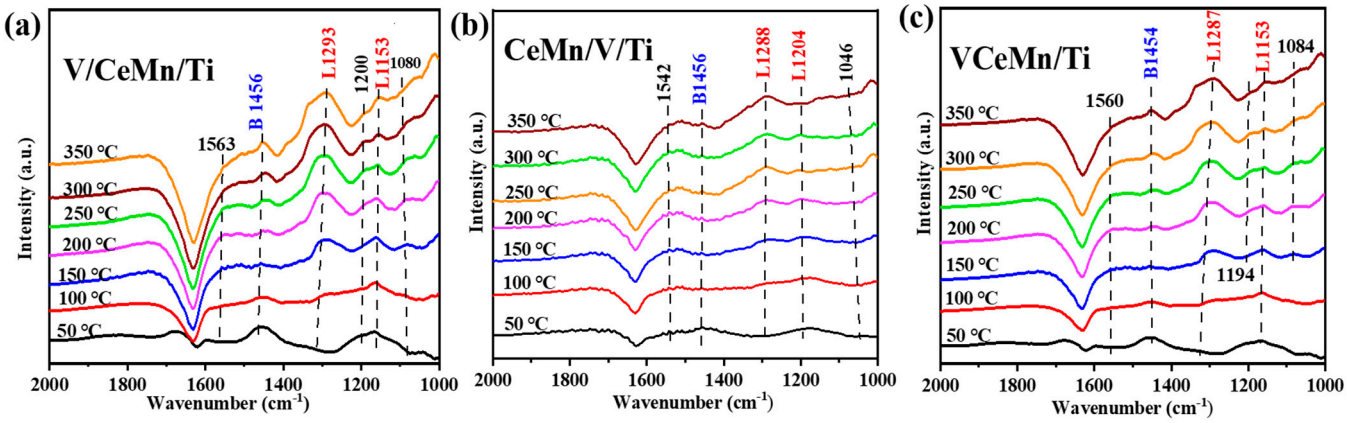

Figure 9. In situ DRIFTS spectra of NH_3 adsorption–desorption: (**a**) V/CeMn/Ti, (**b**) CeMn/V/Ti, and (**c**) VCeMn/Ti.

2.7.2. NO + O_2 Co-Adsorption

Figure 10 displays the in situ DRIFTS spectra of the adsorbed species for the co-adsorption of NO + O_2 on the catalysts, and the presence of adsorbed NO_2 species (~1602 cm^{-1}), bidentate nitrate (1570–1578 cm^{-1}), and NO_2^-/NO_3^- (1217–1370 cm^{-1}, ~1078 cm^{-1}) was shown. The peaks for chelated nitrite and bridged nitrate overlapped [52]. The intensity of bidentate nitrate and monodentate nitrate initially increased and then decreased as the temperature increased. In contrast, the intensity of the nitrate peak increased with the increase in the temperature, which showed that nitrite was steady at 350 °C. The

V/CeMn/Ti catalyst produced more bridged nitrate and bidentate nitrate species than the CeMn/V/Ti and VCeMn/Ti catalysts did. Thus, by combining the benefits of Ce (Mn) species, the V/CeMn/Ti catalyst's adsorption capacity for NO and O_2 was significantly improved, which led to a substantial quantity of nitrogen oxide being adsorbed onto the catalyst surface.

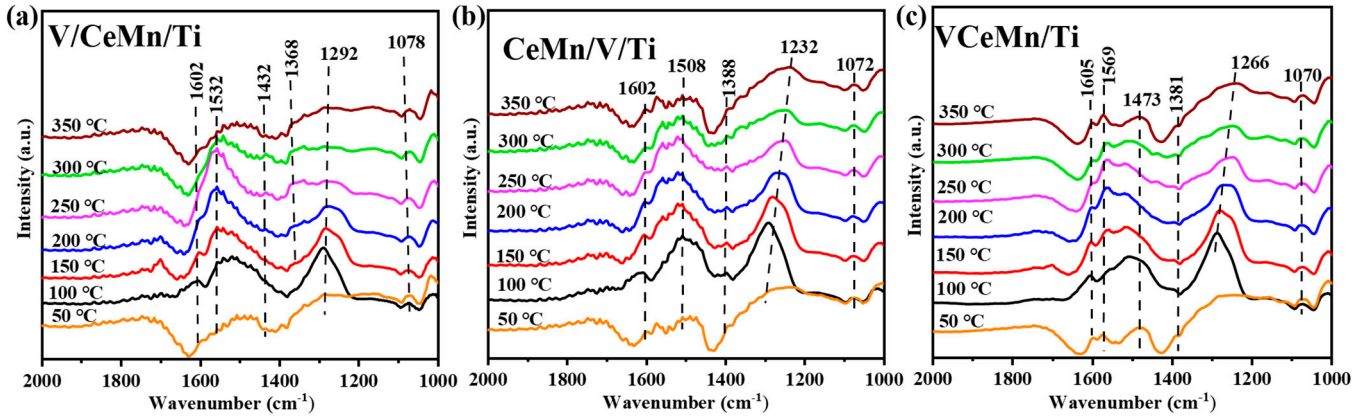

Figure 10. In situ DRIFTS spectra for the catalysts used in the co-adsorption of NO + O_2: (**a**) V/CeMn/Ti, (**b**) CeMn/V/Ti, and (**c**) VCeMn/Ti.

2.7.3. NH_3 + NO + O_2 Co-Adsorption

The catalysts' reaction mechanism was investigated through in situ DRIFTS of NH_3 + NO + O_2 co-adsorption. As shown in Figure 11, adsorbed NO_2 species (~1602 cm^{-1}), bidentate nitrate (~1548 cm^{-1}), -NH_2 species formed through the coordination of NH_3 to L-acid (1540 cm^{-1}), NH_4^+ ions, and monodentate nitrite (1435 cm^{-1}–1442 cm^{-1}) adsorbed on B-acid sites were present. The NH_3 species were found to be adsorbed on L-acid sites at ~1212 cm^{-1} and ~1289 cm^{-1}. Overlapping peaks of NH_2^- and NO_2^-/NO_3^- were also detected at 1352 cm^{-1}, along with NH_4NO_2 at 1078 cm^{-1} [23,50,51,53]. The strength of NH_4^+ adsorbed on the B-acid sites in the V/CeMn/Ti catalyst increased and then decreased with the increase in the temperature, indicating that the B-acid sites were primarily involved in the catalytic reaction of NH_3-SCR at low temperatures. The intensity of NH_3 adsorbed at the L-acid site increased as the temperature increased, which was because the NH_3 from the strong L-acid was chiefly desorbed at high temperatures and participated in the mega-temperature SCR reaction. The NO_2 peak decreased as the temperature increased and disappeared when 200 °C was exceeded, indicating that NO_2 primarily participated in the catalytic reaction at low temperatures. The peak intensities of bridging nitrate (NO_3^-), NH_2^-, and NO_2^- species remained constant throughout the whole process, suggesting their involvement in the catalytic reaction. The above results suggested that the active V species were exposed to the external surface of the catalyst, inducing more acid sites, particularly B-acid sites. The strength of NH_3 adsorption on the L-acid and B-acid sites of the V/CeMn/Ti catalyst was strongest at 150–300 °C. Similarly, the CeMn/V/Ti catalyst exhibited the strongest band strength at 50–150 °C. Surface acidity was shown to be a crucial factor in improving the low-temperature activity of the NH_3-SCR reaction, which was in agreement with the NO conversion rate (refer to Figure 1). The results showed that the Langmuir–Hinshelwood (L−H) mechanism dominated the NH_3-SCR reaction in the V/CeMn/Ti catalyst system.

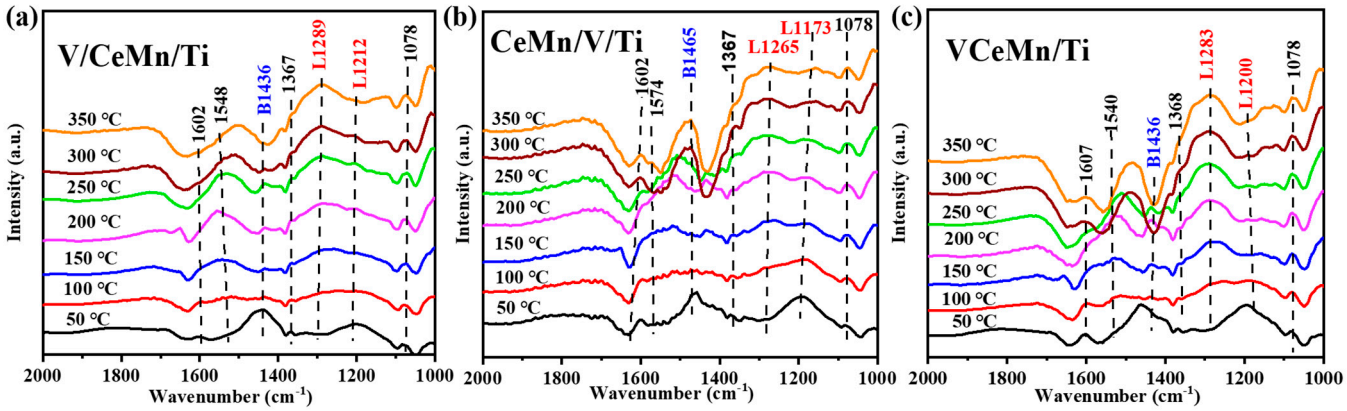

Figure 11. In situ DRIFTS spectra of the catalysts for NH_3 + NO + O_2 co-adsorption: (**a**) V/CeMn/Ti, (**b**) CeMn/V/Ti, and (**c**) VCeMn/Ti.

Based on the in situ DRIFTS analyses, a feasible L−H reaction pathway is proposed in Figures 12 and 13:

$$NH_{3(g)} \rightarrow NH_{3(a)} \quad (3\text{-}1)$$

$$NH_{3(g)} + H^+ \rightarrow NH_4^+{}_{(a)} \quad (3\text{-}2)$$

$$O_{2(g)} \rightarrow 2O_{(\alpha)} \quad (3\text{-}3)$$

$$NO_{(g)} \rightarrow NO_{(a)} \quad (3\text{-}4)$$

$$NO_{(g)} + O_{(\alpha)} \rightarrow NO_{2(a)} \quad (3\text{-}5)$$

$$M^{n+} + NH_{3(a)} \rightarrow M^{(n-1)+} + NH_2^-{}_{(a)} + H^+ \ (M = V, Ce, Mn) \quad (3\text{-}6)$$

$$M^{(n-1)+} + O_{(\alpha)} \rightarrow M^{n+} - O \quad (3\text{-}7)$$

$$M^{n+} - O + NO_{2(a)} \rightarrow M^{(n-1)+} + NO_3^-{}_{(a)} \quad (3\text{-}8)$$

$$M^{(n-1)+} + NO_{2(a)} \rightarrow M^{n+} + NO_2^-{}_{(a)} \quad (3\text{-}9)$$

$$NH_{2(co)} + NO_{(a)} \rightarrow N_2 + H_2O \quad (3\text{-}10)$$

$$NH_4^+{}_{(a)} + NO_{2(a)} \rightarrow NH_4NO_2 \rightarrow N_2 + H_2O \ (L\text{-}H) \quad (3\text{-}11)$$

$$NH_{3(a)} + NO_2^-{}_{(a)} + H^+ \rightarrow NH_4NO_2 \rightarrow N_2 + H_2O \ (L\text{-}H) \quad (3\text{-}12)$$

$$NH_4^+{}_{(a)} + NO_3^-{}_{(a)} \rightarrow NH_4NO_{3(a)} + 2NO_{(a)} + 3NH_{3(a)} \rightarrow N_{2(g)} + H_2O_{(g)} \quad (3\text{-}13)$$

$$NH_4^+{}_{(a)} + NO_2^-{}_{(a)} + NH_2^- + M^{n+} \rightarrow M^{(n-1)+} + N_{2(g)} + H_2O_{(g)} \ (L\text{-}H) \quad (3\text{-}14)$$

"g" for gas phase; "a" for adsorbed species; "$O_{(\alpha)}$" for chemisorbed oxygen

Figure 12. Adsorption and conversion processes of reactive gases in the V/CeMn/Ti catalytic system.

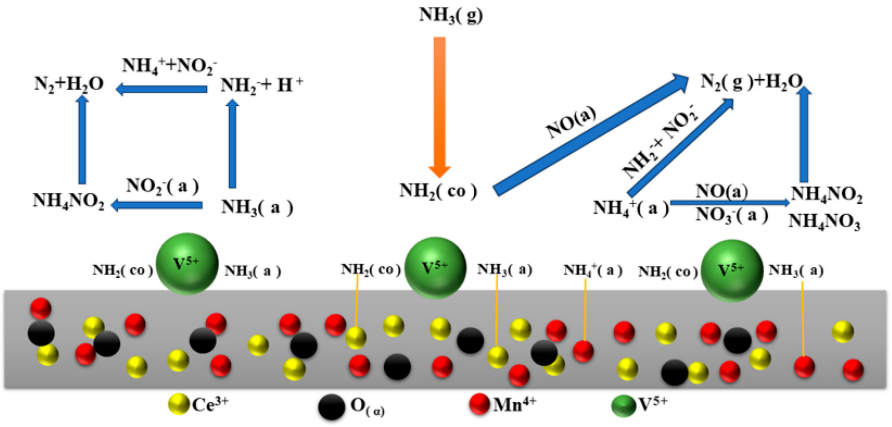

Figure 13. Model of the reaction mechanism (L-H) for different components of the V/CeMn/Ti catalytic system.

3. Experimental Section

3.1. Materials and Methods

V/CeMn/Ti, CeMn/V/Ti, and VCeMn/Ti catalysts were synthesized through stepwise co-impregnation. Taking the V/CeMn/Ti catalyst as an example, firstly, TiO_2 (P25) was immersed in deionized water with completely dissolved $Mn(NO_3)_2$ (10 wt% MnO_2) and $Ce(NO_3)$, as well as $6H_2O$ (5.0 wt% CeO_2), and stirred at room temperature for 1 h. Then, the turbid liquid was dried in an oil bath at 80 °C to remove the solvent and placed in an oven at 110 °C for 12 h. Finally, the solid powder was calcined at 400 °C for 4 h to obtain CeMn/Ti. The same method was used to load the outermost V species; 0.02 g of NH_4VO_3 (1.0 wt% V_2O_5) and 0.045 g of $H_2C_2O_4 \cdot 2H_2O$ were dissolved in 2 mL of water with constant stirring, and oxalic acid was added to promote the dissolution of NH_4VO_3. The solution was immersed in CeMn/Ti and stirred at room temperature for 1 h. Finally, the solid powder was calcined at 400 °C for 4 h to obtain a V/CeMn/Ti catalyst with exposed V species on the outer surface. Similarly, the graded CeMn/V/Ti and VCeMn/Ti catalysts were obtained by changing the order of the impregnants and exposing Ce Mn species and VCeMn on the outer surfaces of the catalysts (wt%:Mn:Ce = 2:1).

3.2. Catalyst Characterization

X-ray diffraction (XRD) was performed using a DX-2700A diffractometer (Dandong Kemait NDT Co.,Ltd , Dandong, China) under Cu–Kα radiation conditions with a voltage of 40 kV and a current of 30 mA. The sweep range was fixed at 10° to 80° with a sweep rate of 10°/min. We obtained N_2 adsorption–desorption isotherms and N_2 pore size distribution curves. The surface area (BET) values were calculated using the Brunauer–Emmet–Teller formula, and the pore size distributions were determined using the Barrett–Joyner–Halenda formula. A scanning electron microscope used to capture the SEM images was a Hitachi S-3400N (Hitachi, Tokyo, Japan). XPS was performed using a Thermo ESCALAB 250Xi+ electron spectrometer (Thermo Fisher Scientific, Waltham, MA USA) equipped with an –Kα X-ray source. C1s (284.8 eV) was used to correct the obtained results.

H_2-TPR was conducted using a Fine-sorb-3010 chemisorption unit under the following conditions: pretreatment at 110 °C for 30 min in N_2 atmosphere, pre-adsorption of 7 vol% H_2 in Ar equilibrium gas for 30 min at room temperature, and a programmed temperature increase to 500 °C at a ramp-up rate of 10 °C/min. Raman spectrometry was carried out at room temperature using a Renishaw in-via reflection spectrometer fitted with an opto-microscope.

NH_3 Program Thermal Desorption (NH_3-TPD) was conducted using a Fine-sorb-3010 chemisorption unit, and the experimental parameters were the following: The pretreatment involved exposing the sample to a N_2 atmosphere at a temperature of 300 °C for a duration of 60 min. Pre-adsorption was achieved by introducing an NH_3 atmosphere (5 vol% NH_3, N_2 as equilibrium gas) at room temperature for 60 min.

In situ diffuse reflectance infrared Fourier transform spectroscopy (DRIFTS) was performed using a Nicolet IS50 spectrometer (Thermo Fisher Scientific, Waltham, MA USA) with a resolution of 4 cm^{-1} and 32 scans. The catalysts were first pre-treated in an N_2 atmosphere at 110 °C for 30 min and then cooled to room temperature to collect the background spectra. Reaction gases were introduced, and a start-up program was automatically programmed for the unit to heat up and record spectra under the following reaction conditions: NH_3 (500 ppm), NO + O_2 (NO = 500 ppm, O_2 = 5 vol%), NH_3 + NO + O_2 (NH_3 = 500 ppm, NO = 500 ppm, O_2 = 5 vol%).

NH_3-SCR activity tests were performed in a fixed-bed reactor, as were H_2O and SO_2 resistance tests, and the exhaust gas concentrations were recorded using an FGA10 flue gas analyzer. Gas conditions: NO = NH_3 = 500 ppm, O_2 = 5 vol%, H_2O = 5 vol%, SO_2 = 50 ppm. Reaction conditions: 40–60 mesh sample particles, and the N_2-pretreated catalyst at 110 °C

adsorbed the reaction gas for 60 min at room temperature. NO_x conversion and N_2 selectivity were determined with the following equations:

$$\text{NO conversion } (\%) = \frac{[NO]_{in} - [NO]_{out}}{[NO]_{in}} \times 100\,\% \quad (1)$$

$$N_2 \text{ selectivity } (\%) = \left(\frac{1 - 2[N_2O]_{out}}{([NO_x]_{in} - [NO_x]_{out}) + ([NH_3]_{in} - [NH_3]_{out})} \right) \times 100\,\% \quad (2)$$

The subscripts "in" and "out" indicate the inlet (before the NH_3-SCR reactor) and outlet (after the NH_3-SCR reactor) gas concentrations of NO, respectively.

4. Conclusions

This study explored the effects of catalysts on NH_3-SCR performance by exposing different active ingredients. The NH_3-SCR properties of the V/CeMn/Ti catalyst were markedly better than those of the CeMn/V/Ti and VCeMn/Ti catalysts, and this catalyst also had a wider operating temperature range. In the V/CeMn/Ti catalyst, Mn and Ce facilitated electron transfer during the catalytic removal of NO_x, while V, as an ancillary species, oxidated NO to NO_2, increasing the number of active species and acidic sites. Furthermore, V was able to protect the active components of Mn and Ce by covering their outer surfaces and preventing interactions with SO_2. This resulted in a stronger tolerance for H_2O + SO_2 while also increasing the number of surface acidic sites, adsorbed nitrites, and nitrate-attached ammonia species, thus facilitating the SCR reaction process. In situ DRIFTS studies showed that the V/CeMn/Ti catalyst followed the L-H mechanism.

Supplementary Materials: The following supporting information can be downloaded at: https://www.mdpi.com/article/10.3390/catal14020131/s1, Figure S1. (a) N_2 adsorption–desorption isotherms; (b) BJH pore size distribution curves; Figure S2. SEM images of catalysts: (a) V/CeMn/Ti; (b) CeMn/V/Ti; (c) VCeMn/Ti.

Author Contributions: S.G.: Conceptualization, Investigation, Methodology, Formal analysis, Writing—original draft, Data curation. C.H.: Resources, Formal analysis, Validation, Visualization. X.H.: Validation, Formal analysis, Software, Visualization. Q.Q.: Software, Visualization, Resources. D.M.: Formal analysis, Software. C.L.: Validation, Formal analysis. Y.Y.: Validation, Visualization. L.D.: Funding acquisition, Supervision. B.L.: Funding acquisition, Project administration, Supervision. All authors have read and agreed to the published version of the manuscript.

Funding: This work was supported by the National Natural Science Foundation of China (No. 22265002 and 22062002).

Data Availability Statement: The data presented in this study are available on request from the corresponding author.

Conflicts of Interest: The authors declare that they have no known competing financial interests or personal relationships that could have appeared to influence the work reported in this paper.

References

1. Han, L.; Cai, S.; Gao, M.; Hasegawa, J.Y.; Wang, P.; Zhang, J.; Shi, L.; Zhang, D. Selective Catalytic Reduction of NO_x with NH_3 by Using Novel Catalysts: State of the Art and Future Prospects. *Chem. Rev.* **2019**, *119*, 10916–10976. [CrossRef] [PubMed]
2. Chu, B.; Ma, Q.; Liu, J.; Ma, J.; Zhang, P.; Chen, T.; Feng, Q.; Wang, C.; Yang, N.; Ma, H.; et al. Air Pollutant Correlations in China: Secondary Air Pollutant Responses to NO_x and SO_2 Control. *Environ. Sci. Technol. Lett.* **2020**, *7*, 695–700. [CrossRef]
3. Wu, X.; Yu, X.; He, X.; Jing, G. Insight into Low-Temperature Catalytic NO Reduction with NH_3 on Ce-Doped Manganese Oxide Octahedral Molecular Sieves. *J. Phys. Chem. C* **2019**, *123*, 10981–10990. [CrossRef]
4. Forzatti, P. Present status and perspectives in de-NO_x SCR catalysis. *Appl. Catal. A Gen.* **2001**, *222*, 221–236. [CrossRef]
5. Xu, J.; Chen, G.; Guo, F.; Xie, J. Development of wide-temperature vanadium-based catalysts for selective catalytic reducing of NO_x with ammonia: Review. *Chem. Eng. J.* **2018**, *353*, 507–518. [CrossRef]

6. Andana, T.; Rappé, K.G.; Gao, F.; Szanyi, J.; Pereira-Hernandez, X.; Wang, Y. Recent advances in hybrid metal oxide–zeolite catalysts for low-temperature selective catalytic reduction of NO_x by ammonia. *Appl. Catal. B Environ.* **2021**, *291*, 120054. [CrossRef]
7. Resitoglu, I.A.; Keskin, A. Hydrogen applications in selective catalytic reduction of NO_x emissions from diesel engines. *Int. J. Hydrogen Energy* **2017**, *42*, 23389–23394. [CrossRef]
8. Vuong, T.H.; Radnik, J.; Rabeah, J.; Bentrup, U.; Schneider, M.; Atia, H.; Armbruster, U.; Grünert, W.; Brückner, A. Efficient $VO_x/Ce_{1-x}Ti_xO_2$ Catalysts for Low-Temperature NH_3-SCR: Reaction Mechanism and Active Sites Assessed by in Situ/Operando Spectroscopy. *ACS Catal.* **2017**, *7*, 1693–1705. [CrossRef]
9. Chen, Z.; Wu, X.; Ni, K.; Shen, H.; Huang, Z.; Zhou, Z.; Jing, G. Molybdenum-decorated V_2O_5–WO_3/TiO_2: Surface engineering toward boosting the acid cycle and redox cycle of NH_3-SCR. *Catal. Sci. Technol.* **2021**, *11*, 1746–1757. [CrossRef]
10. Beck, B.; Harth, M.; Hamilton, N.G.; Carrero, C.; Uhlrich, J.J.; Trunschke, A.; Shaikhutdinov, S.; Schubert, H.; Freund, H.-J.; Schlögl, R.; et al. Partial oxidation of ethanol on vanadia catalysts on supporting oxides with different redox properties compared to propane. *J. Catal.* **2012**, *296*, 120–131. [CrossRef]
11. Boningari, T.; Smirniotis, P.G. Impact of nitrogen oxides on the environment and human health: Mn-based materials for the NO_x abatement. *Curr. Opin. Chem. Eng.* **2016**, *13*, 133–141. [CrossRef]
12. Deng, S.; Meng, T.; Xu, B.; Gao, F.; Ding, Y.; Yu, L.; Fan, Y. Advanced MnO_x/TiO_2 Catalyst with Preferentially Exposed Anatase {001} Facet for Low-Temperature SCR of NO. *ACS Catal.* **2016**, *6*, 5807–5815. [CrossRef]
13. Boningari, T.; Ettireddy, P.R.; Somogyvari, A.; Liu, Y.; Vorontsov, A.; McDonald, C.A.; Smirniotis, P.G. Influence of elevated surface texture hydrated titania on Ce-doped Mn/TiO_2 catalysts for the low-temperature SCR of NO under oxygen-rich conditions. *J. Catal.* **2015**, *325*, 145–155. [CrossRef]
14. Zhang, D.; Zhang, L.; Shi, L.; Fang, C.; Li, H.; Gao, R.; Huang, L.; Zhang, J. In situ supported MnO_x–CeO_x on carbon nanotubes for the low-temperature selective catalytic reduction of NO with NH_3. *Nanoscale* **2013**, *5*, 1127. [CrossRef] [PubMed]
15. Jiang, L.; Liu, Q.; Ran, G.; Kong, M.; Ren, S.; Yang, J.; Li, J. V_2O_5-modified Mn-Ce/AC catalyst with high SO_2 tolerance for low-temperature NH_3-SCR of NO. *Chem. Eng. J.* **2019**, *370*, 810–821. [CrossRef]
16. Yu, C.; Huang, B.; Dong, L.; Chen, F.; Yang, Y.; Fan, Y.; Yang, Y.; Liu, X.; Wang, X. Effect of Pr/Ce addition on the catalytic performance and SO_2 resistance of highly dispersed MnO_x /SAPO-34 catalyst for NH_3-SCR at low temperature. *Chem. Eng. J.* **2017**, *316*, 1059–1068. [CrossRef]
17. Qi, G.; Yang, R.T.; Chang, R. MnO_x-CeO_2 mixed oxides prepared by co-precipitation for selective catalytic reduction of NO with NH_3 at low temperatures. *Appl. Catal. B Environ.* **2004**, *51*, 93–106. [CrossRef]
18. Wang, L.; Huang, B.; Su, Y.; Zhou, G.; Wang, K.; Luo, H.; Ye, D. Manganese oxides supported on multi-walled carbon nanotubes for selective catalytic reduction of NO with NH_3: Catalytic activity and characterization. *Chem. Eng. J.* **2012**, *192*, 232–241. [CrossRef]
19. Li, J.; Liu, H.; Qin, Q.; Zhu, J.; Chu, B.; Sun, Y.; Mo, D.; Dong, L.; Li, B. Functional distinction of different components in SmCeMn/Ti catalytic system for NH_3-SCR. *Appl. Surf. Sci.* **2023**, *636*, 157775. [CrossRef]
20. Liu, J.; Li, X.; Zhao, Q.; Ke, J.; Xiao, H.; Lv, X.; Liu, S.; Tadé, M.; Wang, S. Mechanistic investigation of the enhanced NH_3-SCR on cobalt-decorated Ce-Ti mixed oxide: In situ FTIR analysis for structure-activity correlation. *Appl. Catal. B Environ.* **2017**, *200*, 297–308. [CrossRef]
21. Chen, L.; Li, R.; Li, Z.; Yuan, F.; Niu, X.; Zhu, Y. Effect of Ni doping in $Ni_xMn_{1-x}Ti_{10}$ (x = 0.1–0.5) on activity and SO_2 resistance for NH_3-SCR of NO studied with in situ DRIFTS. *Catal. Sci. Technol.* **2017**, *7*, 3243–3257. [CrossRef]
22. Ye, D.; Qu, R.; Zheng, C.; Cen, K.; Gao, X. Mechanistic investigation of enhanced reactivity of NH_4HSO_4 and NO on Nb- and Sb-doped VW/Ti SCR catalysts. *Appl. Catal. A Gen.* **2018**, *549*, 310–319. [CrossRef]
23. Xie, S.; Li, L.; Jin, L.; Wu, Y.; Liu, H.; Qin, Q.; Wei, X.; Liu, J.; Dong, L.; Li, B. Low temperature high activity of M (M = Ce, Fe, Co, Ni) doped M-Mn/TiO_2 catalysts for NH_3-SCR and in situ DRIFTS for investigating the reaction mechanism. *Appl. Surf. Sci.* **2020**, *515*, 146014. [CrossRef]
24. Zhang, L.; Qu, H.; Du, T.; Ma, W.; Zhong, Q. H_2O and SO_2 tolerance, activity and reaction mechanism of sulfated Ni–Ce–La composite oxide nanocrystals in NH_3-SCR. *Chem. Eng. J.* **2016**, *296*, 122–131. [CrossRef]
25. Goodman, A.L.; Li, P.; Usher, C.R.; Grassian, V.H. Heterogeneous Uptake of Sulfur Dioxide On Aluminum and Magnesium Oxide Particles. *J. Phys. Chem. A* **2001**, *105*, 6109–6120. [CrossRef]
26. Zong, L.; Zhang, G.; Zhao, H.; Zhang, J.; Tang, Z. One pot synthesized CeO_2-WO_3-TiO_2 catalysts with enriched TiO_2 (0 0 1) facets for selective catalytic reduction of NO with NH_3 by evaporation-induced self-assembly method. *Chem. Eng. J.* **2018**, *354*, 295–303. [CrossRef]
27. Wang, X.; Shi, Y.; Li, S.; Li, W. Promotional synergistic effect of Cu and Nb doping on a novel Cu/Ti-Nb ternary oxide catalyst for the selective catalytic reduction of NO_x with NH_3. *Appl. Catal. B Environ.* **2018**, *220*, 234–250. [CrossRef]
28. Li, L.; Zhang, L.; Ma, K.; Zou, W.; Cao, Y.; Xiong, Y.; Tang, C.; Dong, L. Ultra-low loading of copper modified TiO_2/CeO_2 catalysts for low-temperature selective catalytic reduction of NO by NH_3. *Appl. Catal. B Environ.* **2017**, *207*, 366–375. [CrossRef]
29. Cheng, X.; Zhang, X.; Su, D.; Wang, Z.; Chang, J.; Ma, C. NO reduction by CO over copper catalyst supported on mixed CeO_2 and Fe_2O_3: Catalyst design and activity test. *Appl. Catal. B Environ.* **2018**, *239*, 485–501. [CrossRef]
30. Zhang, G.; Han, W.; Zhao, H.; Zong, L.; Tang, Z. Solvothermal synthesis of well-designed ceria-tin-titanium catalysts with enhanced catalytic performance for wide temperature NH_3-SCR reaction. *Appl. Catal. B Environ.* **2018**, *226*, 117–126. [CrossRef]

31. Zhao, X.; Huang, L.; Li, H.; Hu, H.; Hu, X.; Shi, L.; Zhang, D. Promotional effects of zirconium doped CeVO $_4$ for the low-temperature selective catalytic reduction of NO_x with NH_3. *Appl. Catal. B Environ.* **2016**, *183*, 269–281. [CrossRef]
32. He, G.; Lian, Z.; Yu, Y.; Yang, Y.; Liu, K.; Shi, X.; Yan, Z.; Shan, W.; He, H. Polymeric vanadyl species determine the low-temperature activity of V-based catalystsfor the SCR of NO_x with NH_3. *Sci. Adv.* **2018**, *4*, eaau4637. [CrossRef] [PubMed]
33. Jia, X.; Liu, H.; Zhang, Y.; Chen, W.; Tong, Q.; Piao, G.; Sun, C.; Dong, L. Understanding the high performance of an iron-antimony binary metal oxide catalyst in selective catalytic reduction of nitric oxide with ammonia and its tolerance of water/sulfur dioxide. *J. Colloid Interface Sci.* **2021**, *581*, 427–441. [CrossRef] [PubMed]
34. Fan, Z.; Wang, Z.; Shi, J.-W.; Gao, C.; Gao, G.; Wang, B.; Wang, Y.; Chen, X.; He, C.; Niu, C. Charge-redistribution-induced new active sites on (0 0 1) facets of α-Mn_2O_3 for significantly enhanced selective catalytic reduction of NO by NH_3. *J. Catal.* **2019**, *370*, 30–37. [CrossRef]
35. Zhou, X.; Huang, X.; Xie, A.; Luo, S.; Yao, C.; Li, X.; Zuo, S. V_2O_5-decorated Mn-Fe/attapulgite catalyst with high SO_2 tolerance for SCR of NO_x with NH_3 at low temperature. *Chem. Eng. J.* **2017**, *326*, 1074–1085. [CrossRef]
36. Jia, B.; Guo, J.; Luo, H.; Shu, S.; Fang, N.; Li, J. Study of NO removal and resistance to SO_2 and H_2O of MnO/TiO_2, MnO/ZrO_2 and MnO/ZrO_2–TiO_2. *Appl. Catal. A Gen.* **2018**, *553*, 82–90. [CrossRef]
37. Fang, D.; Xie, J.; Hu, H.; Yang, H.; He, F.; Fu, Z. Identification of MnO species and Mn valence states in MnO/TiO_2 catalysts for low temperature SCR. *Chem. Eng. J.* **2015**, *271*, 23–30. [CrossRef]
38. Zhang, P.; Sun, Y.; Su, W.; Wei, Y.; Liu, J. Low-temperature selective catalytic reduction of NO with NH_3 over Ni–Mn–O_x catalysts. *RSC Adv.* **2016**, *6*, 107270–107277. [CrossRef]
39. Wu, Z.; Jin, R.; Liu, Y.; Wang, H. Ceria modified MnO_x/TiO_2 as a superior catalyst for NO reduction with NH_3 at low-temperature. *Catal. Commun.* **2008**, *9*, 2217–2220. [CrossRef]
40. Liu, S.-W.; Guo, R.-T.; Sun, X.; Liu, J.; Pan, W.-G.; Shi, X.; Wang, Z.-Y.; Liu, X.-Y.; Qin, H. Selective catalytic reduction of NO_x over Ce/$TiZrO_x$ catalyst: The promoted K resistance by $TiZrO_x$ support. *Mol. Catal.* **2019**, *462*, 19–27. [CrossRef]
41. Cai, S.; Zhang, D.; Zhang, L.; Huang, L.; Li, H.; Gao, R.; Shi, L.; Zhang, J. Comparative study of 3D ordered macroporous $Ce_{0.75}Zr_{0.2}M_{0.05}O_{2-}\delta$(M = Fe, Cu, Mn, Co) for selective catalytic reduction of NO with NH_3. *Catal. Sci. Technol.* **2014**, *4*, 93–101. [CrossRef]
42. Yu, J.; Si, Z.; Chen, L.; Wu, X.; Weng, D. Selective catalytic reduction of NO by ammonia over phosphate-containing $Ce_{0.75}Zr_{0.25}O_2$ solids. *Appl. Catal. B Environ.* **2015**, *163*, 223–232. [CrossRef]
43. Pappas, D.K.; Boningari, T.; Boolchand, P.; Smirniotis, P.G. Novel manganese oxide confined interweaved titania nanotubes for the low-temperature Selective Catalytic Reduction (SCR) of NO_x by NH_3. *J. Catal.* **2016**, *334*, 1–13. [CrossRef]
44. Zhang, L.; Zhang, D.; Zhang, J.; Cai, S.; Fang, C.; Huang, L.; Li, H.; Gao, R.; Shi, L. Design of meso-TiO_2@MnO_x–CeO_x/CNTs with a core–shell structure as DeNO$_x$ catalysts: Promotion of activity, stability and SO_2-tolerance. *Nanoscale* **2013**, *5*, 9821. [CrossRef] [PubMed]
45. Zhang, L.; Li, L.; Cao, Y.; Yao, X.; Ge, C.; Gao, F.; Deng, Y.; Tang, C.; Dong, L. Getting insight into the influence of SO_2 on TiO_2/CeO_2 for the selective catalytic reduction of NO by NH_3. *Appl. Catal. B Environ.* **2015**, *165*, 589–598. [CrossRef]
46. Chen, H.; Xia, Y.; Huang, H.; Gan, Y.; Tao, X.; Liang, C.; Luo, J.; Fang, R.; Zhang, J.; Zhang, W.; et al. Highly dispersed surface active species of Mn/Ce/TiW catalysts for high performance at low temperature NH_3-SCR. *Chem. Eng. J.* **2017**, *330*, 1195–1202. [CrossRef]
47. Devaiah, D.; Smirniotis, P.G. Effects of the Ce and Cr Contents in Fe–Ce–Cr Ferrite Spinels on the High-Temperature Water–Gas Shift Reaction. *Ind. Eng. Chem. Res.* **2017**, *56*, 1772–1781. [CrossRef]
48. Damma, D.; Boningari, T.; Smirniotis, P.G. High-temperature water-gas shift over Fe/Ce/Co spinel catalysts: Study of the promotional effect of Ce and Co. *Mol. Catal.* **2018**, *451*, 20–32. [CrossRef]
49. Chen, Y.; Zhang, Z.; Liu, L.; Mi, L.; Wang, X. In situ DRIFTS studies on MnO nanowires supported by activated semi-coke for low temperature selective catalytic reduction of NO with NH_3. *Appl. Surf. Sci.* **2016**, *366*, 139–147. [CrossRef]
50. Xie, S.; Qin, Q.; Liu, H.; Jin, L.; Wei, X.; Liu, J.; Liu, X.; Yao, Y.; Dong, L.; Li, B. MOF-74-M (M = Mn, Co, Ni, Zn, MnCo, MnNi, and MnZn) for Low-Temperature NH_3-SCR and In Situ DRIFTS Study Reaction Mechanism. *ACS Appl. Mater. Interfaces* **2020**, *12*, 48476–48485. [CrossRef]
51. Liu, L.; Xu, K.; Su, S.; He, L.; Qing, M.; Chi, H.; Liu, T.; Hu, S.; Wang, Y.; Xiang, J. Efficient Sm modified Mn/TiO_2 catalysts for selective catalytic reduction of NO with NH_3 at low temperature. *Appl. Catal. A Gen.* **2020**, *592*, 117413. [CrossRef]
52. Liu, S.; Wang, H.; Wei, Y.; Zhang, R. Core-shell structure effect on CeO_2 and TiO_2 supported WO_3 for the NH_3-SCR process. *Mol. Catal.* **2020**, *485*, 110822. [CrossRef]
53. Wang, B.; Wang, M.; Han, L.; Hou, Y.; Bao, W.; Zhang, C.; Feng, G.; Chang, L.; Huang, Z.; Wang, J. Improved Activity and SO_2 Resistance by Sm-Modulated Redox of MnCeSmTiO_x Mesoporous Amorphous Oxides for Low-Temperature NH_3-SCR of NO. *ACS Catal.* **2020**, *10*, 9034–9045. [CrossRef]